Supplementary Information

Photothermal Effect of Carbon Quantum Dots Enhanced Photoelectrochemical Water Splitting of Hematite Photoanodes

Xiaoqin Hu,[a] Jing Huang,[a] Feifan Zhao,[a] Ping Yi,[a] Bing He,[a] Yang Wang,[a] Tao Chen,[c] Yihuang Chen,*[b] Zhen Li,*[a] and Xueqin Liu*[a]

[a] Engineering Research Center of Nano-Geomaterials of Ministry of Education, Faculty of Materials Science and Chemistry, China University of Geosciences, Wuhan, Hubei, 430074, China

[b] College of Chemistry and Materials Engineering, Wenzhou University, Wenzhou, Zhejiang 325035, China

[c] Hubei Key Laboratory of Radiation Chemistry and Functional Materials, Hubei University of Science and Technology, Xianning, Hubei, 437100, China

*Corresponding author (X. Liu): E-mail: liuxq@cug.edu.cn

Contents

Ⅰ. Experimental section

Preparation of Fe_2O_3/TiO_2 Photoanode

The Fe_2O_3/TiO_2 NRs were fabricated according to a reported procedure but with modifications. Firstly, Iron chloride hexahydrate ($FeCl_3 \cdot 6H_2O$, 3.243 g) and urea (CON_2H_4, 0.72 g) were dissolved in distilled water (80 mL), magnetic continuous stirred for 30 minutes to formed homogeneous solution. Then, the mixing solution was transferred to a Teflon-lined stainless-steel autoclave (100 mL volume), where six clean TiO_2/FTO substrates were placed in advance. Subsequently, the autoclave was sealed and heated at 100 °C for 6 h. After the reaction, the sample was washed with distilled water and ethanol and dried with N_2. Finally, it was annealed in air at 550 °C for 2 h at a heating rate of 3 °C min^{-1}, and then at 750 °C for 10 min at the heating rate of 10 °C min^{-1}.

Preparation of CQDs/Fe_2O_3/TiO_2 Photoanode

The Fe_2O_3/TiO_2 NRs were soaked in 2 mg/mL carbon quantum dots solution stored in a constant temperature fridge for different time (24 h, 24 h, 48 h, 60 h, 72 h). The CQDs/Fe_2O_3/TiO_2 NRs were obtained after removed, rinsed with distilled water and nitrogen gun dry.

Preparation of Co-Pi/CQDs/Fe_2O_3/TiO_2 Photoanode

The Co-Pi cocatalyst decorated the CQDs/Fe_2O_3/TiO_2 NRs by a constant voltage deposition in a typical three-electrode cell. CQDs/Fe_2O_3/TiO_2 NRs, Ag/AgCl and Pt foil were regarded as working electrode, reference electrode and counter electrode, respectively. The electrolyte was consisted of 0.25 mM cobalt nitrate hexahydrate and 0.1 M potassium phosphate buffer solution. 0.2 V vs. Ag/AgCl was applied for different time (10 s, 30 s, 50 s, 70 s and 90 s) under the AM1.5G irradiation (100 mW cm^{-2}) from the front of sample. The resulting Co-Pi/CQDs/Fe_2O_3/TiO_2 NRs was withdrawn and rinsed with distilled water.

Characterizations

The morphologies of samples were characterized by field emission scanning electron microscopy (FESEM, Hitachi Global, SU8010) and transmission electron microscopy (TEM, Philips CM12 TEM/STEM, Holland Philips). Energy dispersive X-ray (EDX) spectroscopy coupled to TEM was used to analyze the composition of the samples. The crystalline structures of the as-prepared photoanodes were detected by powder X-ray diffraction (XRD, Bruker AXS, D8 Focus) with Cu Ka radiation (λ = 1.54056 °A). X-ray photoelectron spectra (XPS) was measured on a Thermo VG Escalab 220i XL and the binding energies were calibrated with respect to the residual C (1s) peak at 285.0 eV. Raman spectra were measured on a micro-Raman spectrometer (Renishaw, laser wavelength 532 nm). The ultraviolet-visible visible diffuse reflectance spectroscopy (UV-Vis, Perkin-Elmer Lambda 35) was employed to investigate the optical properties of samples. The photoluminescence spectrum (PL, RF-5301PC fluorospectrophotometer) was recorded with an excitation wavelength of 320 nm.

Photoelectrochemical experiments

Photoelectrochemical measurements were evaluated in 1 M NaOH aqueous solution (pH 13.6) by a three-electrode configuration connected to an electrochemical station (CHI 660E, Chenhua, Shanghai, China). Pt foil, Ag/AgCl with saturated KCl solution and the as-prepared samples were acted as counter electrode, reference electrode and working electrode, respectively. The light source was simulated sunlight from a 150 W xenon solar simulator (96000, Newport Corp.) through a solar filter with a measured intensity equivalent to standard AM1.5 sunlight (100 mW cm^{-2}) at the back of sample face. The near infrared laser of 808 nm (MDL-H-808-5W, DANGER) was used to provide thermal energy for samples. The measured potentials vs. Ag/AgCl were converted to the reversible hydrogen electrode (RHE) scale using the relationship $E_{RHE} = E_{Ag/AgCl} + 0.059*pH + E^{\theta}_{Ag/AgCl}$, where $E_{Ag/AgCl}$ is the experimentally measured potential and $E^{\theta}_{Ag/AgCl}$ = 0.197 V vs. Ag/AgCl at 25 °C.

Photocurrent vs. voltage (*J-V*) characteristics was measured with the positive scanning rate of 50 mV/s. Incident photon-to-electron conversion efficiency (IPCE) spectra were measured using a Newport Xe lamp (150 W) coupled with a

monochromator (Ceaulight, CEL-QPCE3000) at an applied potential of 1.23 V_{RHE}. Electrochemical Impedance Spectroscopy (EIS) measurements were investigated by sweeping the frequency interval 0.01-10^5 Hz with an amplitude of 10 mV at the open-circle potential under illumination of simulated solar light. The Mott-Schottky dates were measured with a sinusoidal voltage perturbation of 10 mV amplitude at 1 kHz in dark conditions. Photoelectrochemical H_2 evolution was studied in 1.0 M NaOH after saturation with Ar gas for 60 min. Evolved H_2 gas was collected and measured according to the standard H_2 evolution curve by a gas chromatograph (GC-2014C, Shimadzu).

Ⅱ. Calculation

Applied bias photon-to-current efficiency (ABPE)

Faradaic efficiency, the applied bias photon-to-current efficiency (ABPE) was caclulated by following equation (S1):

$$ABPE(\%) = \frac{I \times (1.23 - V_{bais})}{P_{light}} \times 100\ \% \qquad \text{(S1)}$$

where I is the photocurrent density (mA cm^{-2}), V_{bias} is the applied potential (V_{RHE}), P_{light} is the incident illumination power density (100 mW cm^{-2}).

Incident photon-to-current efficiency (IPCE)

IPCE was performed under monochromatic irradiation from a 300 W Xenon arc lamp coupled with a monochromator (Ceaulight, CEL-QPCE3000) at 1.23 V_{RHE} according to the equation (S2):

$$IPCE\ (\%) = \frac{1240 * J_{ph}(\lambda)}{P\ (\lambda)\ * \lambda} \times 100\ \% \qquad \text{(S2)}$$

in which $J_{ph}(\lambda)$,□λ, and P(λ) are photocurrent density (mA cm^{-2}), wavelength of light (nm), power density of monochromatic light (mW cm^{-2}) which was measured by a calibrated Si detector, respectively.

Calculation of carrier concentration (N_D)

In the M-S plot, the flat band potential of the photoelectrode is estimated according to

following equation (S3):

$$\frac{1}{C^2} = \frac{2}{e\varepsilon\varepsilon_0 N_D}\left[\left(E - E_{FB}\right) - \frac{\kappa T}{e}\right] \quad \text{(S3)}$$

in which C is the space charge capacitance, e = 1.60 × 10^{-19} C is the electron charge, ε is the relative dielectric constant of hematite (ε□= 80) , ε_0□is the vacuum permittivity (8.85×10^{-12} F/m), N_D is the charge donor density (cm^{-3}), E is the electrode applied potential, E_{FB} is the flat band potential, k is the Boltzmann's constant (1.38×10^{-23} J/K) and T is the absolute temperature (K). In addition, the slopes determined from the analysis of M-S plots were applied to calculate the carrier density (N_D) by the following equation (S4):

$$N_D = -\left(\frac{2}{e\alpha\varepsilon\varepsilon_0}\right)\left(\frac{d\left(1/C^2\right)}{d\left(U_s\right)}\right)^{-1} \quad \text{(S4)}$$

Calculation of bulk charge separation and surface charge injection efficiency: The measured water splitting photocurrent (J_{H_2O}) can be described as equation (S5):

$$J_{H_2O} = J_{abs} \times \eta_{sep} \times \eta_{inj} \quad \text{(S5)}$$

Where J_{abs} is determined by the integral of the area of the solar spectrum and the light harvesting efficiency (LHE) obtained by UV-Vis spectrum according to formula (S6) and Fig. S8b:

$$\text{LHE} = 1\text{-}10^{-A(\lambda)} \quad \text{(S6)}$$

Where A(λ) is the absorbance at wavelength λ. The obtained result of J_{abs} for FT, CFT and CCFT photoanodes is 10.5, 11.4 and 10.9 mA cm^{-2}, respectively. η_{sep} is the separation efficiency of photogenerated holes that reach the electrode/electrolyte interface without recombining with electrons in the bulk. η_{inj} is the injection efficiency of photogenerated holes from electrode to electrolyte without being recombined with electrons at surface traps. In the presence of hole scavenger Na_2SO_3, the surface recombination of charge carriers can be completely suppressed without influencing the charge separation in the electrode bulk (i.e., η_{inj} = 100%). Thus, the charge separation and charge injection efficiency can be calculated as following

equations (S7 and S8):

$$\eta_{sep}(\%) = \frac{J_{SO^{2-}_3}}{J_{abs}} \quad \text{(S7)}$$

$$\eta_{inj}(\%) = \frac{J_{H_2O}}{J_{SO^{2-}_3}} \quad \text{(S8)}$$

Where J_{H_2O} and $J_{SO^{2-}_3}$ are the photocurrents achieved in the electrolytes of 1 M NaOH and 1 M Na_2SO_3 + 1 M NaOH, respectively.

Electrochemically active surface area: The electrochemically active surface area (ECSA) was estimated from the electrochemical double-layer capacitance. Cyclic voltammograms were performed in 1 M KOH (pH = 13.6) at the scan rate of 40, 60, 80, 100, 120, 140, 160, and 180 mV s-1. Then the electrochemical active surface area was determined by measuring the capacitive current associated with double-layer charging from the scan-rate dependence of CVs. The double layer capacitance (C_{dl}) was estimated by plotting the △J = (Ja - Jc) at 1.0 VRHE against the scan rate. The linear slope is equivalent to twice of the C_{dl}, which can be used to represent the electrochemical active surface area.

Ⅲ. UV-Vis absorption and PL spectra of CQDs solution

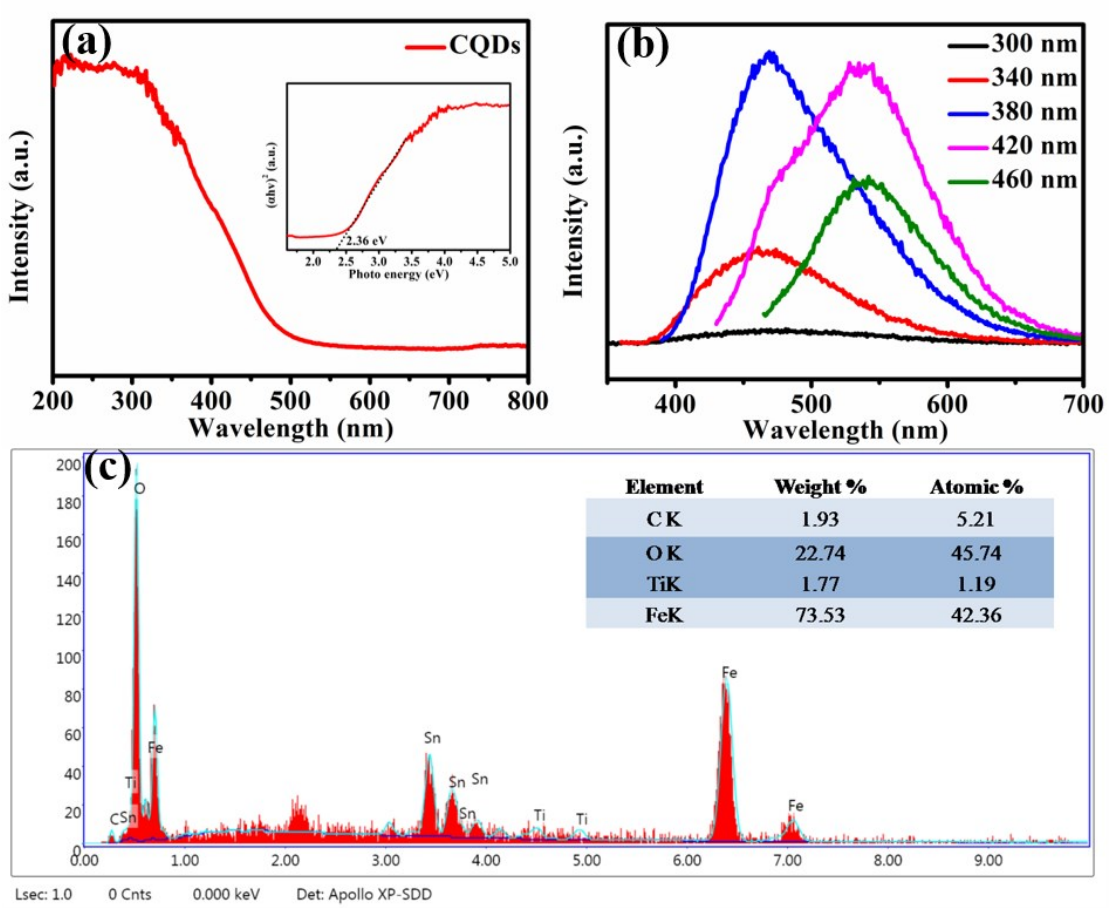

Fig. S1 UV-Vis (a) and PL (b) spectroscopy of CQDs solution. EDS elemental analysis of CFT photoanodes (c). The inset in (a) is the band gap estimation based on the Kubelka-Munk function for CQDs.

Ⅳ. Crystalline phase property of the photoanodes

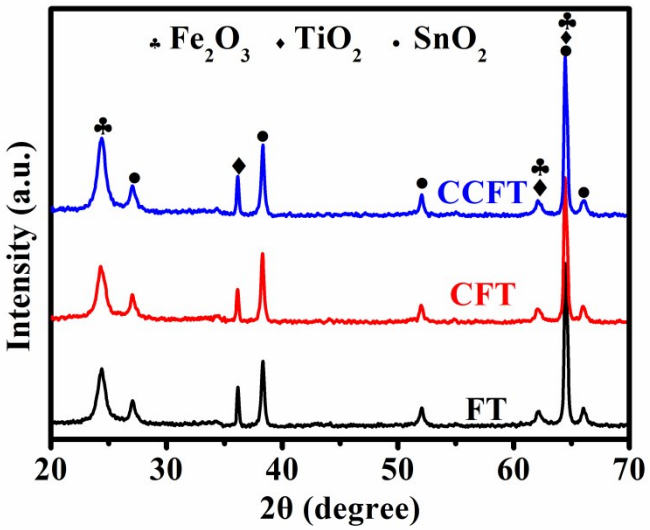

Fig. S2 Powder XRD patterns of FT, CFT and CCFT NRs.

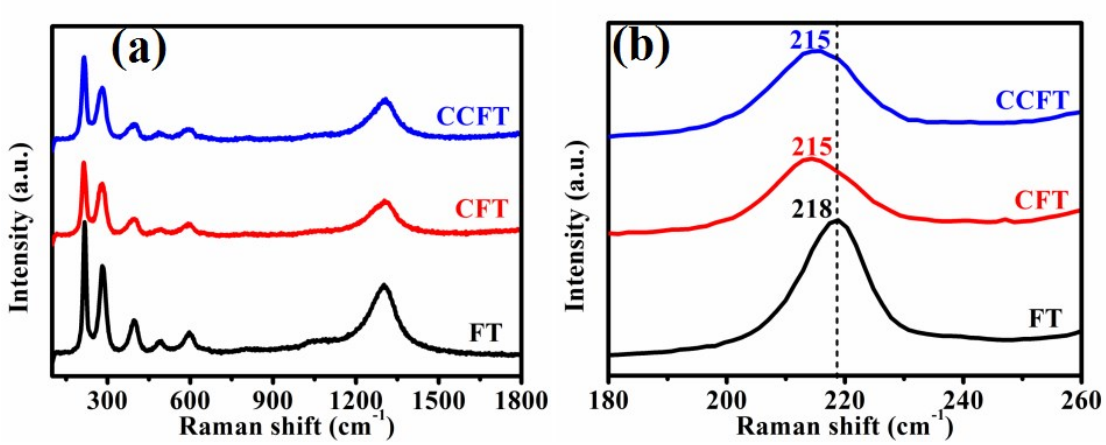

Fig. S3 Raman spectra (a) and the enlarged view for Raman shift range from 180 to 260 cm^{-1} (b) of FT, CFT and CCFT NRs.

Ⅴ. XPS spectra of the photoanode

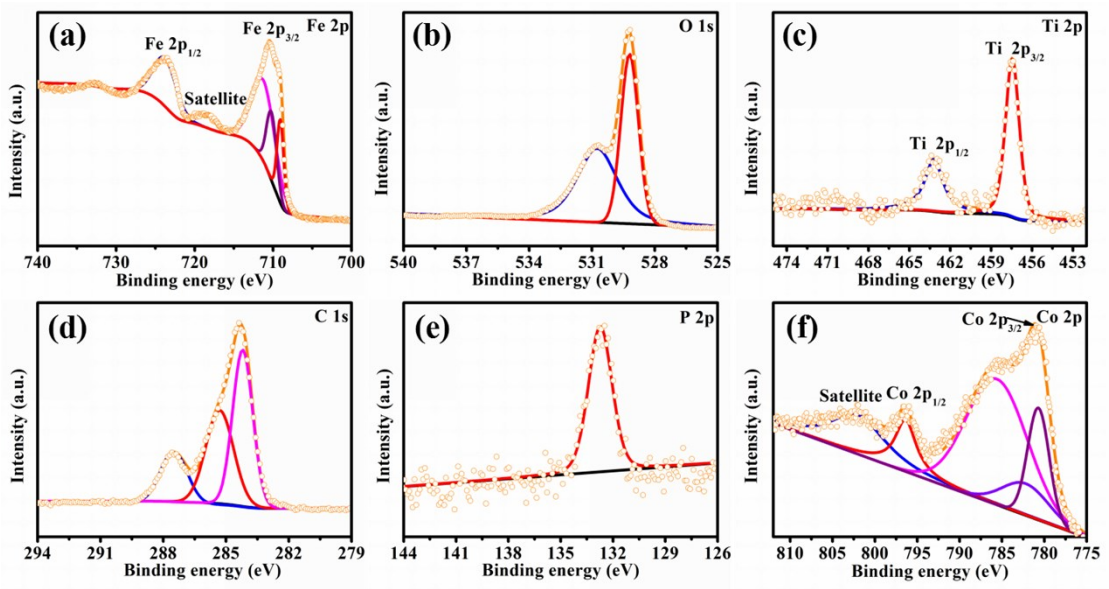

Fig. S4 High resolution XPS spectra of (a) Fe 2p, (b) O 1s, (c) Ti 2p, (d) C 1s, (e) P 2p and (f) Co 2p for the CCFT NRs.

Ⅵ. UV-Vis absorption spectra of the photoanodes

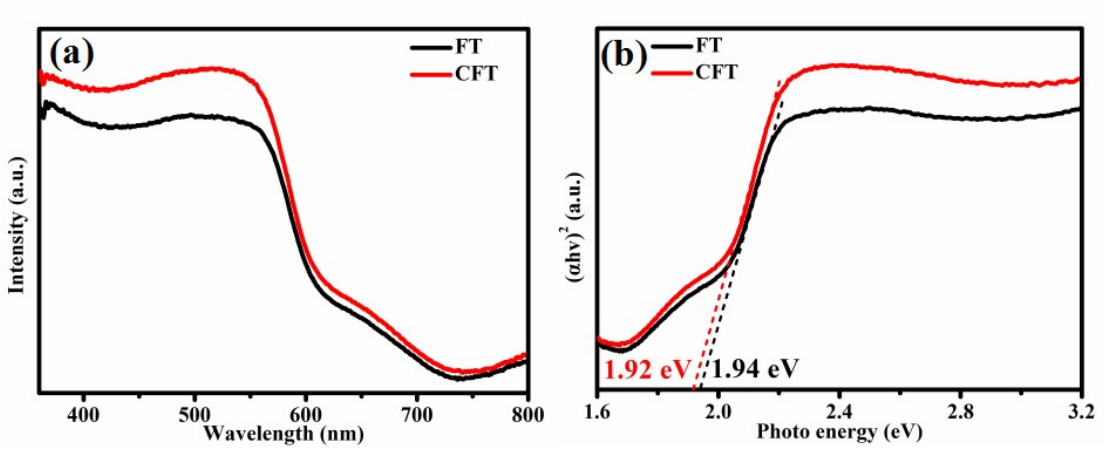

Fig. S5 (a) UV-Vis diffuse reflectance spectra and (b) plots of $(\alpha hv)^2$ *vs*. photon energy for FT, CFT and CCFT NRs samples.

Ⅶ. Mechanism of charge separation for CCFT photoanodes.

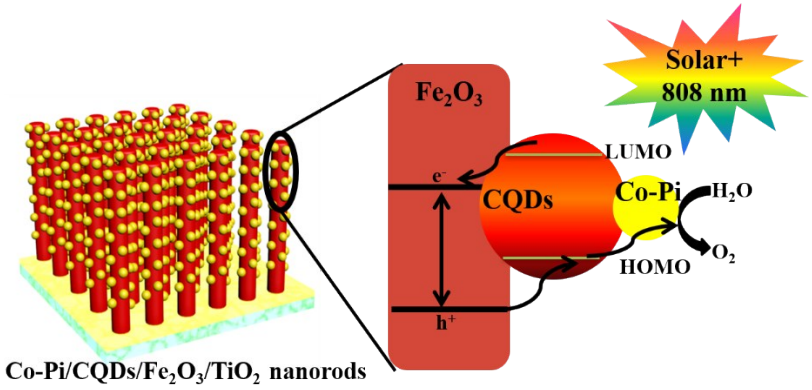

Fig. S6 Mechanism of charge separation for CCFT photoanodes.

Ⅷ. PEC results of the photoanodes with different contents of CODs and Co-Pi

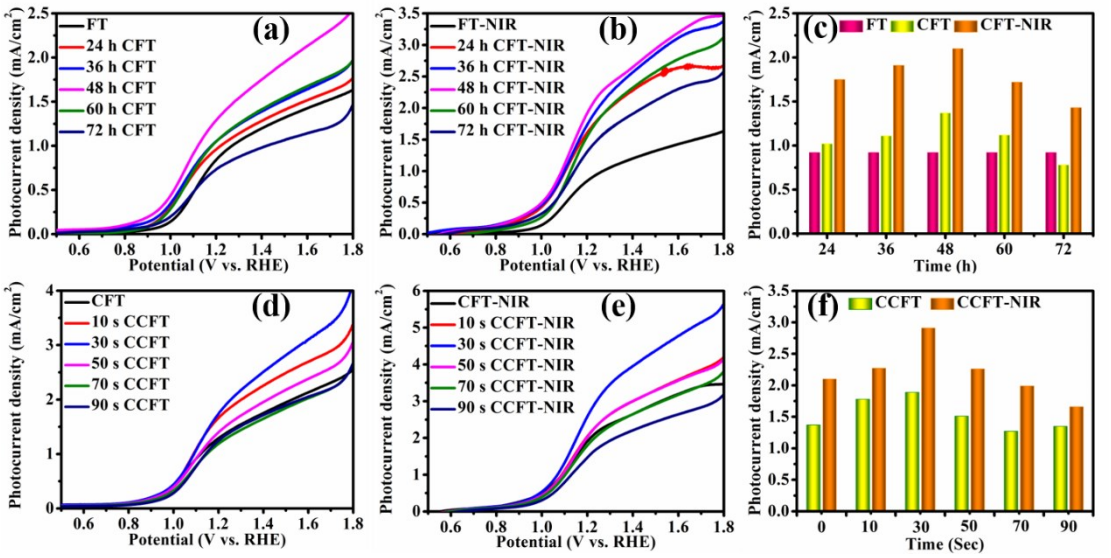

Fig. S7 The effect of CQDs (a-c) and Co-Pi (d-f) deposition contents on the PEC performance of different photoanodes.

Ⅸ. Mott-Schottky (M-S) plots of the photoanodes under light

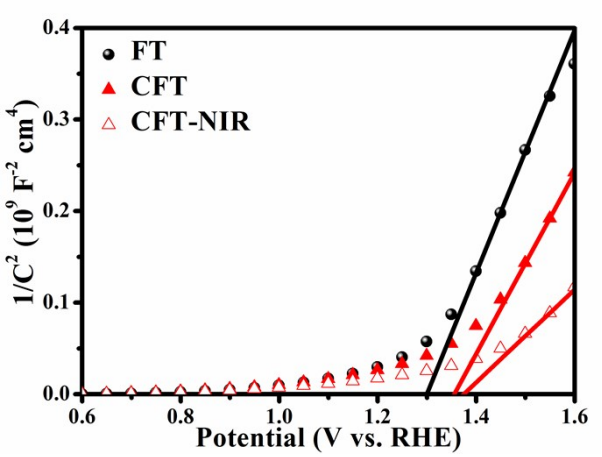

Fig. S8 M-S plots for photoelectrodes measured under the irradiation of AM 1.5G.

X. Cyclic voltammetry (CV) curves of the photoanodes

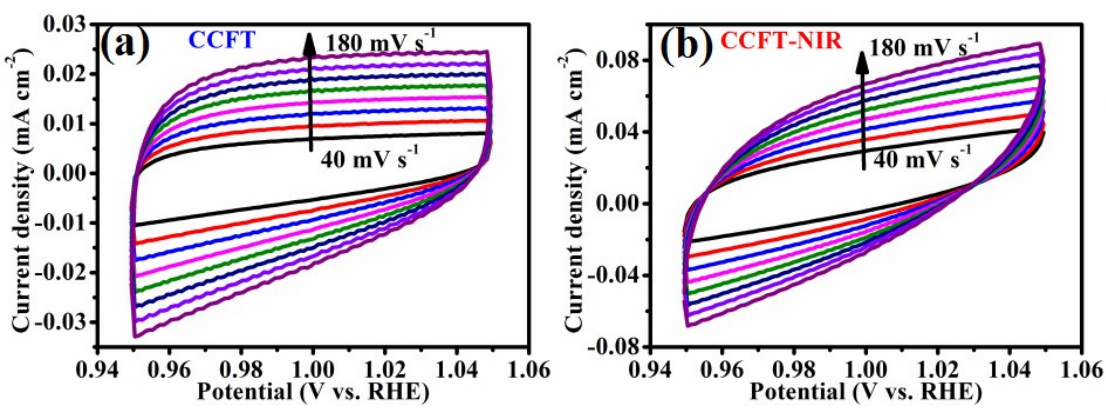

Fig. S9 Voltammograms of the (a) CCFT and (b) CCFT-NIR photoanodes at various scan rates (20-180 mV s^{-1}).

XI. Electron flux and J-V curves of the photoanodes

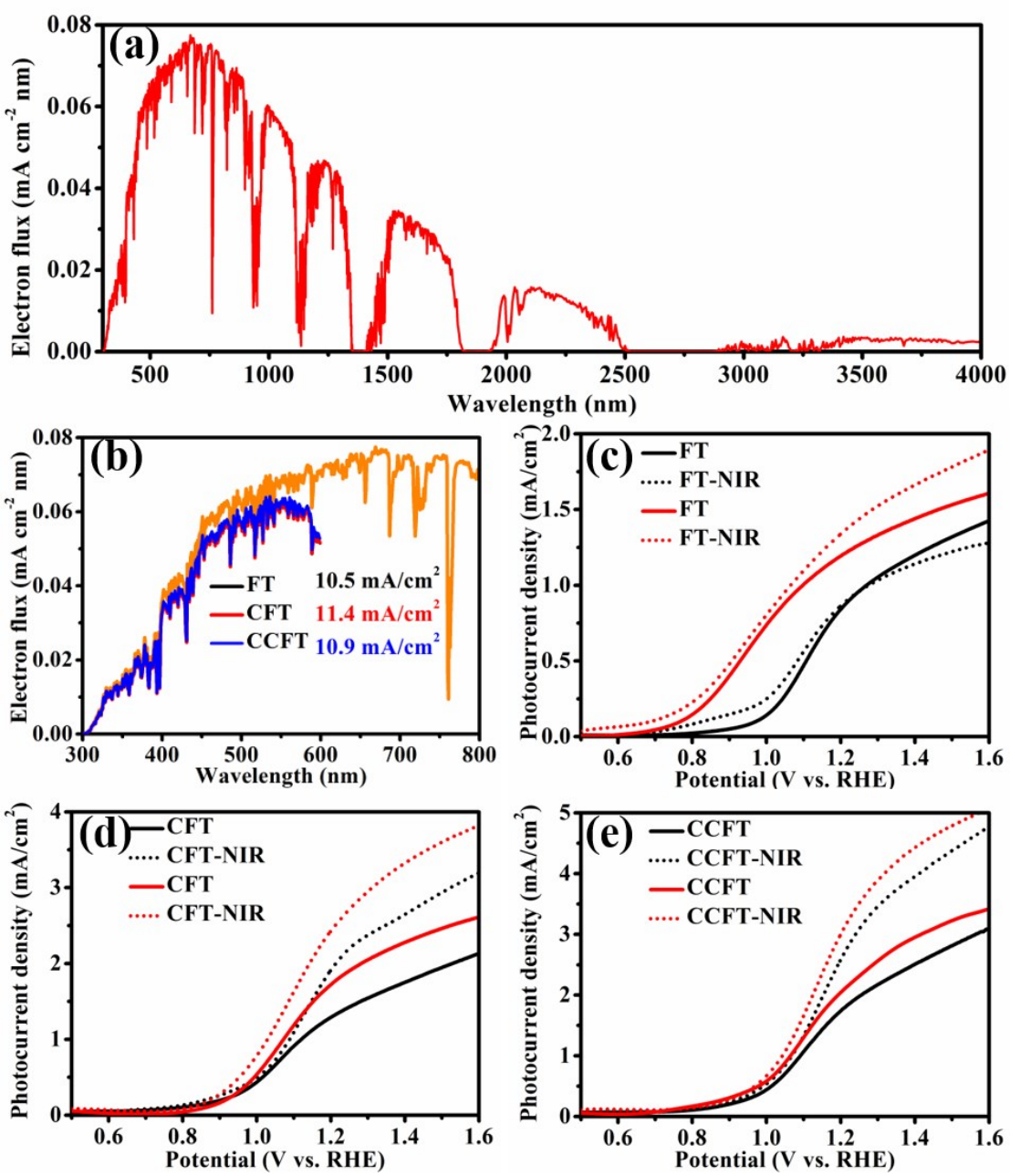

Fig. S10 (a) Electron flux of AM 1.5G solar spectrum. (b) Electron flux of FT, CFT and CCFT. LSV plots of photoanodes in the electrolyte of NaOH (red solid and dashed) and NaOH+Na_2SO_3 (black solid and dashed) for (c) FT, (d) CFT, and (e) CCFT, respectively.

Ⅻ. Comparison study of PEC performance

Table S1. A comparison study between the CCFT-NIR photoanode in this work and previously reported Fe_2O_3-based photoanodes toward PEC water splitting.

Photoanode	J (mA cm^{-2}) at 1.23 V_{RHE}	Stability	Electrolyte	Ref.
Sn-Fe_2O_3/$NiCo_2S_4$	1.51 mA cm^{-2}	—	1 M KOH	[1]
NiOOH/Fe_2O_3/F-Fe_2O_3	2.48 mA cm^{-2}	2 h	1 M KOH	[2]
Fe_2O_3/Fe_2TiO_5/$FeNiO_x$	2.70 mA cm^{-2}	5 h	1 M KOH	[3]
ITO/Fe_2O_3/Fe_2TiO_5/FeNiOOH	2.20 mA cm^{-2}	2 h	1 M NaOH	[4]
Mg-Fe_2O_3/P-Fe_2O_3	2.40 mA cm^{-2}	2 h	1 M KOH	[5]
Ti-(SiO_x/np-Fe_2O_3)	2.44 mA cm^{-2}	2 h	1 M NaOH	[6]
FeOOH/Fe_2O_3	1.21 mA cm^{-2}	—	1 M NaOH	[7]
C/Ti-Fe_2O_3-Ar	1.32 mA cm^{-2}	—	0.1 M NaOH	[8]
3D Co-Fe_2O_3/$MgFe_2O_4$	3.34 mA cm^{-2}	—	0.01 M Na_2SO_4	[9]
(Sn, Zr)-Fe_2O_3-NiOOH	1.64 mA cm^{-2}	10 h	1 M NaOH	[10]
Ti:Fe_2O_3@GCNN-CQD	3.38 mA cm^{-2}	5 h	1 M KOH	[11]
FeOOH/M:B-doped-Fe_2O_3	2.35 mA cm^{-2}	—	1 M NaOH	[12]
Co-Pi/Co_3O_4/Ti:Fe_2O_3	2.70 mA cm^{-2}	—	1 M KOH	[13]
N_2 treated Fe_2O_3:Ti	2.40 mA cm^{-2}	—	1 M NaOH	[14]
Co-Pi/CQDs/Fe_2O_3/TiO_2-NIR	3.00 mA cm^{-2}	3 h	1 M NaOH	This work

XIII. References

1. S. Seenivasan, M. Hee, K. Do-Heyoung, *Catalysis Today,* 2018**,** DOI: 10.1016/j.cattod.2018.05.045.
2. F. Li, J. Li, L. Gao, Y. Hu, X. Long, S. Wei, C. Wang, J. Jin, J. Ma, *J. Mater. Chem. A.,* 2018, **46**, 23478-23485.
3. C. Li, T. Wang, Z. Luo, S. Liu, J. Gong, *Small,* 2016**, 25**, 3415-3422.
4. P. Tang, H. Xie, C. Ros, L. Han, M. Biset-Peiro´, Y. He, W. Kramer, A. Pe´rez Rodrı´guez, E. Saucedo, J. Ramo´n Gala´n-Mascaro´s, T. Andreu, J. Ramon Morantea, J. Arbiol, *Energy Environ. Sci.,* 2017**, 10**, 2124-2136.
5. F. Li, J. Li, F. Li, L. Gao, X. Long, Y. Hu, C. Wang, S. Wei, J. Jin, J. Ma, *J. Mater. Chem. A.,* 2018, **6**, 13412-13418.
6. H. Ahn, K. Yoon, M. Kwak, J. Jang, *Angew. Chem. Int. Ed.,* 2016**, 55**, 1-6.
7. J. Kim, D. Youn, K. Kang, J. Lee, *Angew. Chem. Int. Ed.,* 2016, **55**, 10854-10858.
8. D. Yan, J. Liu, Z. Shang, H. Luo, *Dalton Trans.,* 2017**, 46**, 10558-10563.
9. Y. Hou, F. Zuo, A. Dagg, P. Feng, *Angew. Chem. Int. Ed.,* 2013, **125**, 1286-1290.
10. A. Tamirat, W. Su, A. Dubale, H. Chena, B. Hwang, *J. Mater. Chem. A.,* 2015, **3**, 5949-5961.
11. S. Yi, J. Yan, Q. Jiang, *J. Mater. Chem. A.,* 2018**, 6**, 9839-9845.
12. H. Ahn, K. Yoon, M. Kwak, J. Park, J. Jang, *ACS Catal.,* 2018, ***8***, 11932-11939.
13. S. Yi, B. Wulan, J. Yan, Q. Jiang, *Adv. Funct. Mater.,* 2019, *1801902*.
14. Z. Wang, X. Mao, P. Chen, M. Xiao, S. Monny, S. Wang, M. Konarova, A. Du, L. Wang, *Angew. Chem. Int. Ed.*, 2019, **58**, 1030-1034.